Available online at www.sciencedirect.com
ScienceDirect
Ceramics International 38 (2012) 495–502
CERAMICS INTERNATIONAL
www.elsevier.com/locate/ceramint

Hydrothermal synthesis of hierarchical hydroxyapatite: Preparation, growth mechanism and drug release property

Li-Xia Yang [a,*], Jia-Jun Yin [b], Lu-Lu Wang [a], Guo-Xiu Xing [a], Ping Yin [a], Quan-Wen Liu [a]

[a] School of Chemistry and Materials Science, Ludong University, Yantai 264025, China
[b] Yantaishan Hospital, Yantai 264001, China

Received 11 May 2011; received in revised form 9 July 2011; accepted 16 July 2011
Available online 26th July 2011

Abstract

Hydroxyapatite (HAP) hierarchical microspheres were synthesized by a facile hydrothermal method using calcium nitrate and ammonium dihydrogen phosphate through controlling complexing agents. The influences of two kinds of complexing agents (potassium sodium tartrate tetrahydrate and trisodium citrate) and reaction time on the morphology of HAP crystals have been investigated. These results indicate that complexing agents have a great influence on the morphology of HAP. When potassium sodium tartrate tetrahydrate was used as complexing agent, HAP flowers were composed of the network of nanosheet building blocks. Well-crystallized HAP dandelions with nanorods radiating from the center can be obtained by the introduction of trisodium citrate. Broader XRD diffraction peaks imply a nanometer scale size. Based on XRD and SEM results, the formation mechanism of HAP crystals has been discussed. The hierarchically structured HAP microspheres were explored as drug carriers. The results indicate that HAP flowers and dandelions showed a favorable sustained release property for ibuprofen; thus, they are very promising for application in drug delivery.

Keywords: A. Powders: chemical preparation; B. Microstructure; D. Apatite

1. Introduction

Hydroxyapatite ($Ca_{10}(PO_4)_6(OH)_2$), as one of the most important inorganic biomaterials, has received long-term attention due to its extensive applications, especially as bone repair and tissue engineering [1–3]. In addition, HAP can be used as chromatography [4], drug delivery agent [5–8] and protein delivery agent [9]. These promising applications have promoted the development for various methods to synthesize HAP crystals. Examples are chemical precipitation approach [10], hydrothermal reaction [11,12], flux synthesis [13], biomimetic method [14] and phase conversion method from different calcium phosphates such as octacalcium phosphate [15], α-tricalcium phosphate [16], brushite [17] or monetite [18]. For example, Tan et al. [10] synthesized water-dispersible hydroxyapatite nanorods by a chemical precipitation of aqueous solutions of calcium nitrate and triammonium phosphate at 90 °C. Neira et al. [11] employed a urea-assisted hydrothermal reaction between $Ca(NO_3)_2$ and $(NH_4)_2HPO_4$ to prepare plate-like, hexagonal prism-like, needle-like and fine-plate-like HAP. Mou and coworkers [15] have synthesized uniform nanorods of hydroxyapatite and reported the transformation from octacalcium phosphate to HAP and its impact on the crystal morphology in a gelatin matrix.

In recent years, scientists have paid more attention to the controlled organization of primary building block units into curved structures across extended dimensions, since the properties of materials are closely correlated to their morphology [19,20]. Formation of highly ordered complex architectures organized by nanostructured building blocks based on spontaneous processes is of great interest for boosting the performance of applications. It has been demonstrated that using surfactants, polymers and complexing agents can be an effective strategy to regulate the crystal growth process. Wang et al. [21] synthesized flower-like porous hydroxyapatite microspheres through poly(styrene sulfonate). Spherical hydroxyapatite crystals were successfully prepared with β-cyclodextrin as template by biomimetic method [22]. However, only limited literatures involved the preparation of hierarchical HAP crystals using complexing agents and drug

* Corresponding author. Tel.: +86 535 6672176; fax: +86 535 6695905.
E-mail address: yanglx2003@163.com (L.-X. Yang).

0272-8842/$36.00
doi:10.1016/j.ceramint.2011.07.033

release property, especially the relationship between morphology and drug release property. Herein, we demonstrated a facile hydrothermal method to prepare HAP microspheres constructed by different building blocks via the introduction of two kinds of complexing agents. The hierarchically structured HAP microspheres were explored as drug carriers. A typical anti-inflammatory drug, ibuprofen (IBU), was used for drug loading, and the release behaviors of ibuprofen in a simulated body fluid (SBF) were studied.

2. Experimental details

2.1. Preparation

All chemicals were of analytical graded reagents and used without further purification. In a typical procedure for the preparation of hydroxyapatite flowers, 0.75 mmol ammonium dihydrogen phosphate ($NH_4H_2PO_4$) and 1.67 mmol urea were dissolved in 15 mL deionized water to form a transparent solution 1. 1.25 mmol calcium nitrate ($Ca(NO_3)_2{\cdot}4H_2O$) and 2.5 mmol potassium sodium tartrate tetrahydrate (PST) were separately dissolved in 7.5 mL deionized water, and then PST solution was quickly added to $Ca(NO_3)_2$ solution, white precipitate occurred immediately. Solution 1 was introduced into this suspension. After vigorously stirring for 2 min, the as-obtained mixing solution was transferred to a Teflon-lined stainless steel autoclave of 50 mL capacity, filled up to 60% of the total volume, sealed, and maintained at 180 °C for 24 h. As the autoclave cooled to room temperature naturally, the precipitates were separated by centrifugation, washed with deionized water and ethanol in sequence, and then dried in air at 60 °C. This sample was denoted as PST-HAP. In another experiment, 0.83 mmol trisodium citrate (TSC) was used to substitute PST as complexing agent to synthesize hydroxyapatite dandelions, while keeping the other conditions the same as the above sample. This sample was denoted as TSC-HAP. PSC-HAP and TSC-HAP samples were calcined at 800 °C for 6 h to investigate high-temperature stability of HAP, these two samples were designated as PSC-HAP-800 and TSC-HAP-800.

2.2. In vitro drug release

The obtained HAP crystals can be used as drug carriers. In present study, two samples including PST-HAP and TSC-HAP with different structures were investigated for drug loading and release. The typical drug loading and in vitro drug release experiments were performed as follows: 3.5 g IBU was dissolved in 50 mL hexane at a concentration of 70 mg/mL. HAP (1.0 g) was added to this solution (50 mL) at room temperature. Standard conical flasks (100 mL capacity) were sealed with ground-in glass stopper to prevent the evaporation of hexane, and then the mixture was shaken at 30 °C at a rate of 160 rpm for 24 h. The shaking device was a desk-type constant temperature oscillator (SHA-CA, China). The sample was centrifuged, washed once using hexane, dried at 60 °C in air and compacted into disks (each disk 0.3 g) by a pressure of 4 MPa. Each disk was immersed into 200 mL of simulated body fluid with pH 7.4 at 37 °C under shaking at a constant rate of 160 rpm. The ibuprofen release medium solution (2 mL) was taken out for UV–vis analysis at 264 nm at given time intervals and replaced with the same volume of fresh SBF which was preheated to 37 °C. The samples of PST-HAP and TSC-HAP with released IBU are denoted as PST-HAP-IBU and TSC-HAP-IBU.

2.3. Characterization

Phase characterization of the as-synthesized products was conducted with X-ray powder diffraction analysis (XRD, Rigaku D/max 2500 VPC) using high-intensity Cu Kα radiation (λ = 1.54178 Å) and a graphite monochromator in the 2θ range from 5° to 80°. Morphology was investigated using scanning electron microscopy (FEI-Sirion 200, Philips, Holland and JSM-5610LV, JEOL, Japan). BET surface area measurement was performed by a surface area analyzer (ASAP 2020, Micro-meritics Corporation, USA). UV–vis absorption spectra were taken on a Shimadzu UV 2550 spectrophotometer.

3. Results and discussion

3.1. Morphology of the obtained products

The phase of the as-prepared sample using PST as complexing agent was examined by XRD. Fig. 1a shows XRD pattern of sample PST-HAP prepared at 180 °C for 24 h. All diffraction peaks in this pattern can be indexed as a single phase of hexagonal hydroxyapatite, which is consistent with the values in the literature (JCPDS No. 09-0432). No other phases were observed. Typical SEM micrographs shown in Fig. 1b–d reveal that the sample was mainly consisted of relatively uniform flower-like structures. The flower-like structure was composed of the network of nanosheet building blocks. The sizes of these flowers were in the range of 5–15 μm, the thicknesses of nanosheets were below 100 nm (Fig. 1d). Brunauer–Emmett–Teller (BET) gas sorptometry measurement revealed that the specific surface area of HAP flowers was 34 m^2/g. The above results demonstrate that HAP with flower-like morphology can be produced using the present synthetic scheme.

When TSC was used as complexing agent, the phase and morphology of the obtained sample were shown in Fig. 2. Single phase of HAP was obtained (Fig. 2a). As one can see from image at low magnification (Fig. 2b), the sample mainly consisted of microspheres with diameters up to 5 μm. Their surface exhibits a dandelion-like morphology as depicted in Fig. 2c and d. HAP ‘‘dandelions’’ comprise numerous one-dimensional nanorods radiating from the center. The diameter of these nanorods is in the range of 30–50 nm. BET gas sorptometry measurement revealed that the specific surface area of HAP dandelions was 101 m^2/g. This result shows that HAP morphology can be influenced by complexing agents in this reaction system.

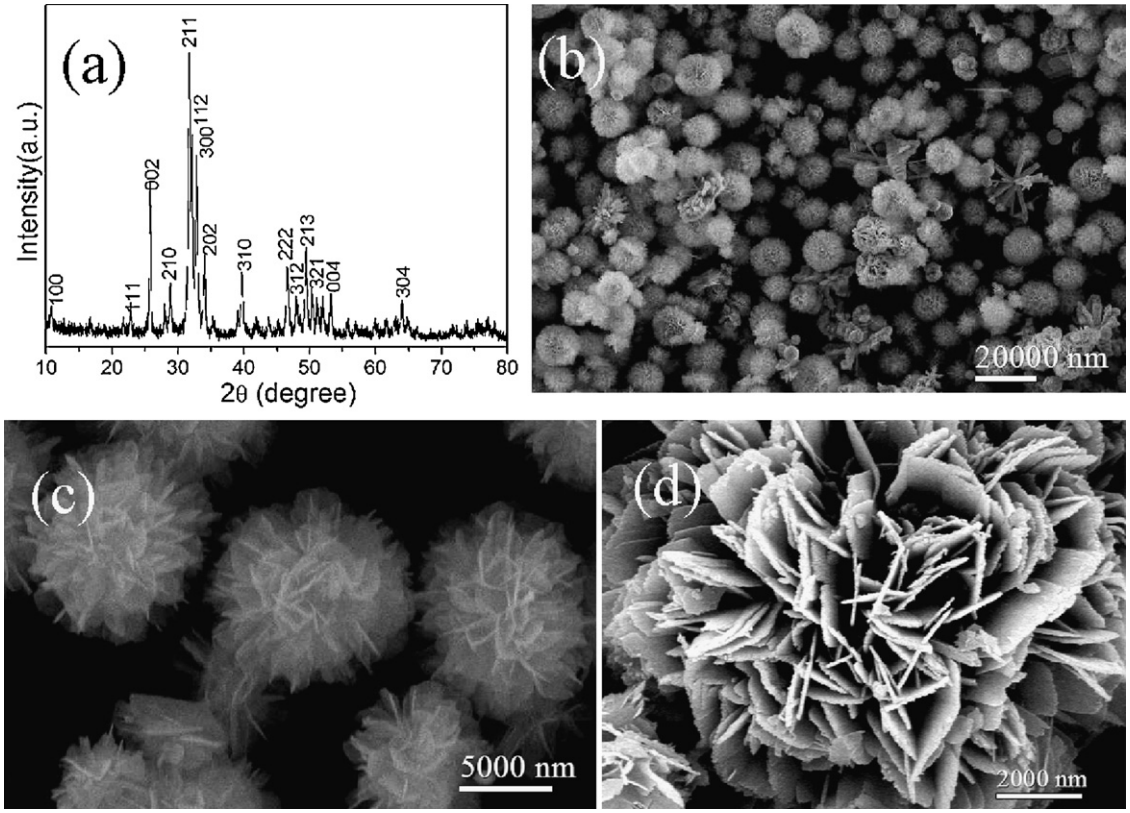

Fig. 1. XRD pattern and SEM images of sample PST-HAP.

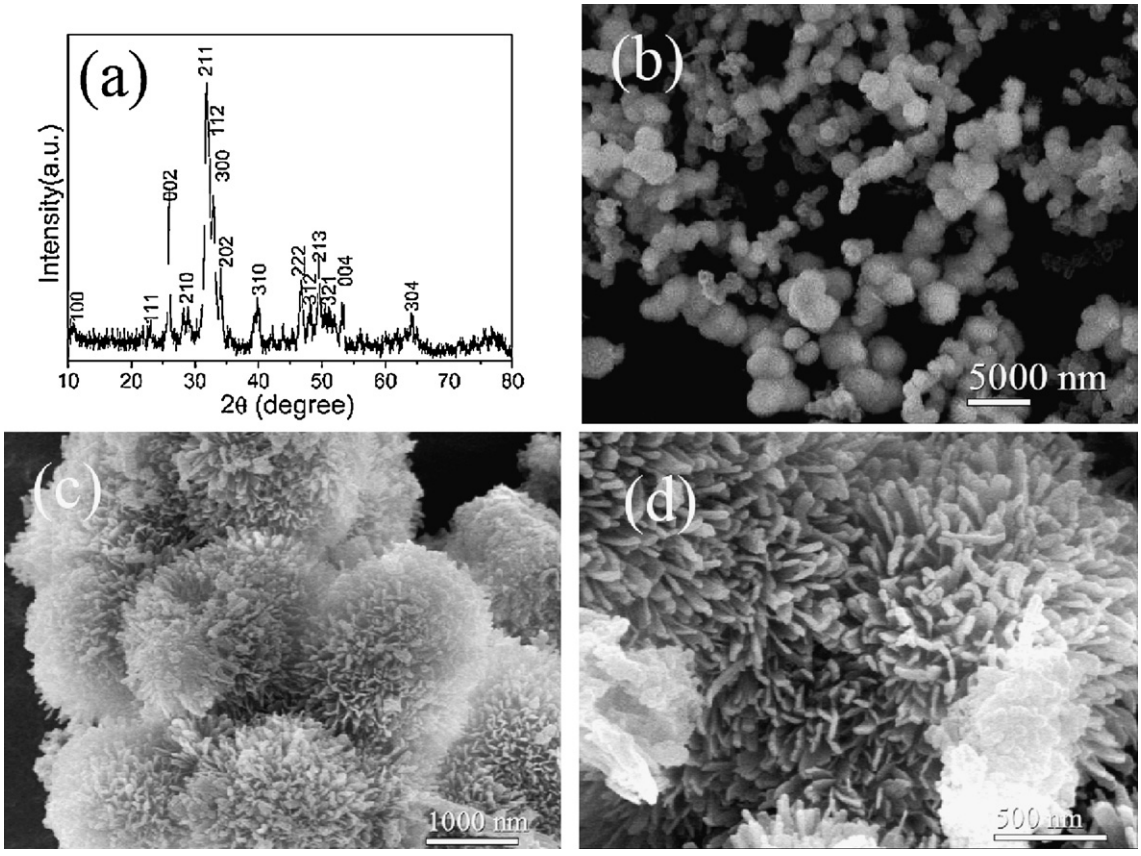

Fig. 2. XRD pattern and SEM images of sample TSC-HAP.

3.2. Formation mechanism

The effect of PST concentration on the morphologies of HAP microspheres was studied. Along with the increase of PST concentration, crystal morphologies of HAP were different. As for the samples in the absence of PST, the sample mainly consisted of HAP nanoribbons. A few of nanoribbon aggregates were observed (Fig. 3a and b). When 0.32 mmol PST was introduced in this system, the product showed a loosely packed flowers constructed by nanoribbons comparing to the sample without PST, as illustrated in Fig. 3c and d. The obtained microspheres had diameters about 30 μm. Interestingly, the nanobuilding units of these microspheres gradually changed from nanoribbons to nanoplates as PST concentration was increased to 2.5 mmol (Fig. 1b–d). Consequently, dense microspheres formed eventually. Hence, we can suggest that PST can influence the formation of flower-like hydroxyapatite.

To examine the influence for HAP crystals after different hydrothermal time, XRD patterns of the products synthesized at 180 °C were measured as shown in Fig. 4. As we stated in the preparation section, white precipitate can be produced after mixing $Ca(NO_3)_2$ and PST. After introducing urea and $NH_4H_2PO_4$ to this precipitate, white precipitate still existed (Fig. 4a). Calcium tartrate seems to be the white product; however, no JCPDS card can support this result. This precursor can be sustained after 1 h of reaction at 180 °C (Fig. 4b). When the hydrothermal time was prolonged to 3 h, hydroxyapatite coexists with the precursor (indicated as *, Fig. 4c). The transformation from precursor to hydroxyapatite cannot complete even after 6 h, as shown in Fig. 4d. The phase of the product still remains as a mixture of precursor and hydroxyapatite. The characteristic peaks displayed in XRD pattern of Fig. 4e are consistent with those of hydroxyapatite (JCPDS No. 09-0432). It took relatively longer time to form a single phase of hydroxyapatite.

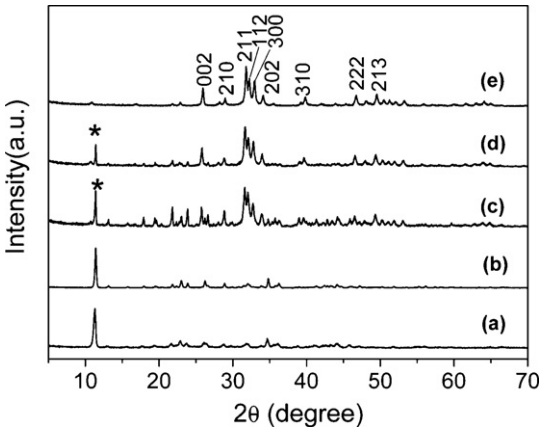

Fig. 4. XRD patterns of sample PST-HAP prepared for different hydrothermal time. (a) 0 h; (b) 1 h; (c) 3 h; (d) 6 h; (e) 12 h.

The influences of reaction time on the morphology were investigated with PST concentration fixed at 2.5 mmol. As displayed in Fig. 5a, before hydrothermal treatment, the precursor showed a sheet-like morphology. In the case of 1 h (Fig. 5b), flowers assembled from nanosheets were observed with dimensions below 10 μm and single nanoribbons coexisted. When the reaction time was increased to 3 h, sample still shows mixed morphologies of nanoribbons and flowers (Fig. 5c). Further prolonging hydrothermal time to 6 h, the morphology of the products remains a mixture of nanoribbons and flowers (Fig. 5d). However, the proportion of flowers seems to be enhanced and individual nanoribbons get decreased. Petals in these flowers were denser than samples prepared at the earlier stages.

XRD patterns and SEM photographs of the products prepared using TSC as complexing agent at 180 °C for different hydrothermal time are shown in Fig. 6. It is clear that

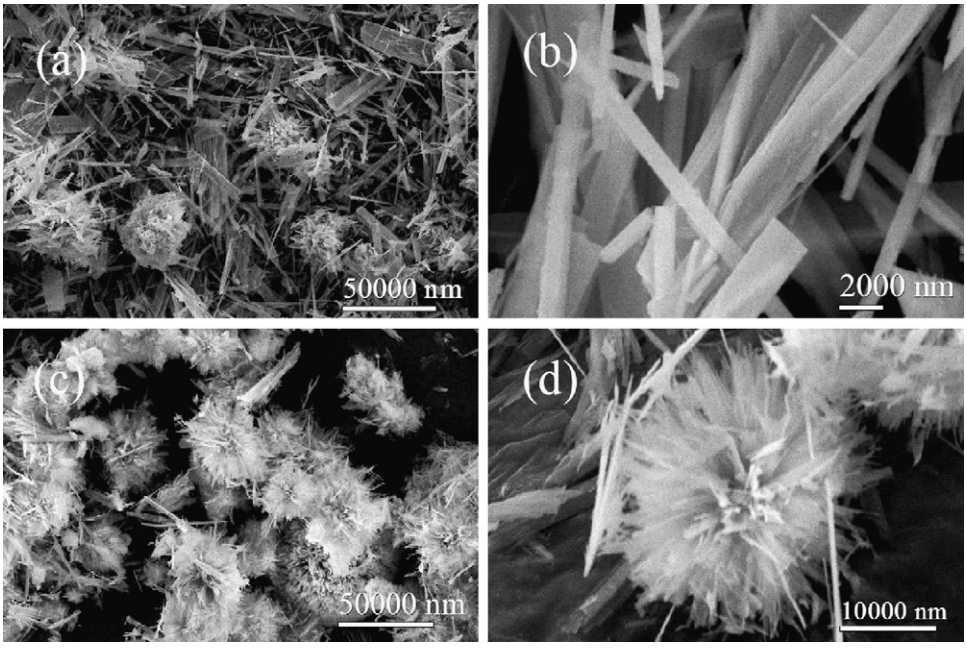

Fig. 3. SEM images of samples with different PST concentrations. (a and b) 0 mmol; (c and d) 0.32 mmol.

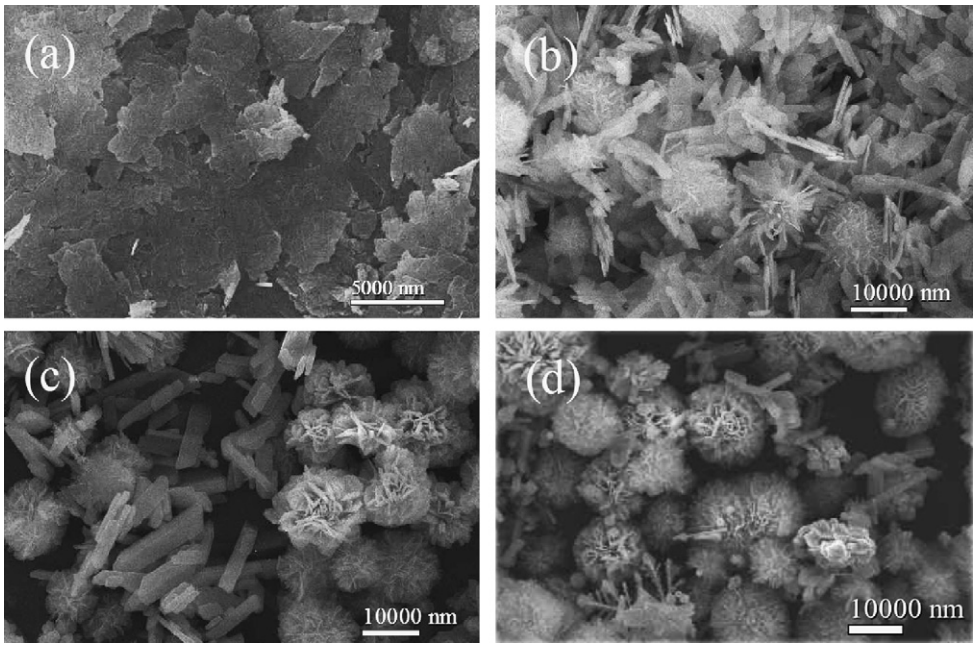

Fig. 5. SEM images of sample PST-HAP prepared for different hydrothermal time. (a) 0 h; (b) 1 h; (c) 3 h; (d) 6 h.

the diffraction peaks of the product had only broad diffraction peaks, which was an indication that the as-formed HAP was poorly crystallized (Fig. 6a). Microspheres formed with diameters in the range of 1–3 μm. The surface of the microspheres was rough (Fig. 6b). As the hydrothermal time prolonged to 3 h, the crystallinity degree of the product was enhanced. Major peaks were identified in comparison with the standard power diffraction data for HAP (JCPDS No. 09-0432).

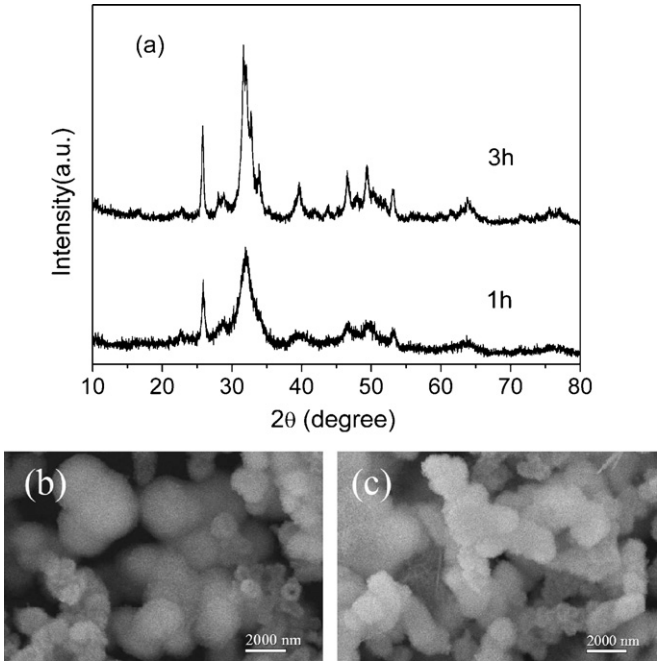

Fig. 6. (a) XRD patterns of sample TSC-HAP prepared for different hydrothermal time; (b) SEM image of sample TSC-HAP prepared for 1 h; (c) SEM image of sample TSC-HAP prepared for 3 h.

However, three most intensive peaks of (2 1 1), (1 1 2) and (3 0 0) between 30° and 35° (2θ) in standard diffraction curve were obscure, which was possibly caused by low crystallinity or nanometer scale size distribution. The microsphere grew slowly with the increase of the reaction time (Fig. 6c). A hydrothermal time of 24 h provided a sufficient driving force to increase crystallinity as shown in Fig. 2a.

On the basis of above structural and morphological analysis, it can be deduced that complexing agent has a great impact on morphology of the final products. In the case of PST complexing agent, the formation of precursor occurred before and after hydrothermal reaction for 1 h. In this period, the sample mainly presents morphology of nanoribbons, only a few flowers can be observed. Further increasing the hydrothermal time to 3 h or even 6 h, respectively, mixed morphology was sustained. However, the proportion of flowers can be greatly enhanced as shown in Fig. 5d. The efforts of PST in our system

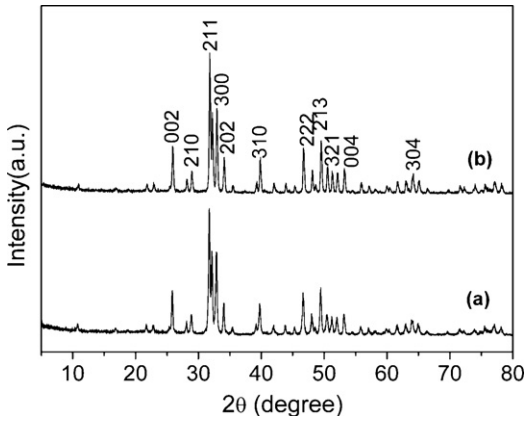

Fig. 7. XRD patterns of different samples after calcination. (a) PST-HAP-800; (b) TSC-HAP-800.

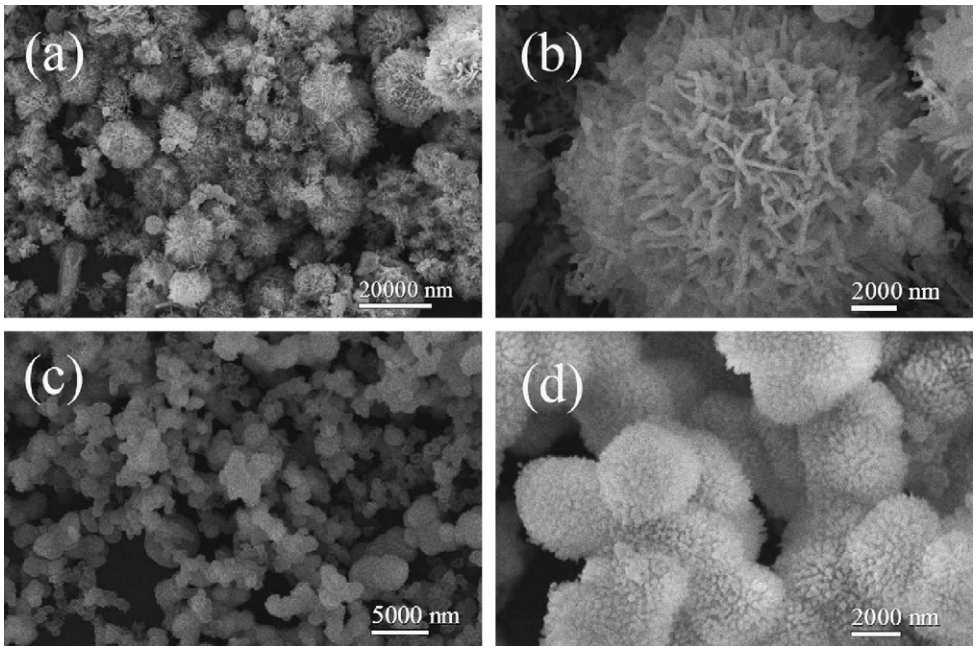

Fig. 8. SEM images of different samples. (a and b) PST-HAP-800; (c and d) TSC-HAP-800.

could be attributed to two aspects: firstly, the formation of precursor precipitation led to less free Ca^{2+} concentration, which avoided the direct chemical precipitation to HAP. Secondly, the transformation from precursor to HAP underwent a period of Ca^{2+} release from precursor nanoribbons to the solution, which can provided enough free Ca^{2+} concentration to precipitate as HAP. In this process, HAP flowers can be obtained from the solution at the expense of the dissolution of precursor. It is worth noting that the dissolution of precursor nanoribbons differed from the decomposition of Ca^{2+}–citrate complex, which were well dispersed in the solution without precipitation. The existence of precursor makes the crystal growth process took place on the interface of solid and liquid. Hence, HAP crystals can exhibit a different morphology to samples using TSC. As for TSC as complexing agent, the existence of Ca^{2+} in solution is in the form of Ca^{2+}–citrate complex and PO_4^{3-} presents as free anion. When the reaction system was hydrothermally treated, Ca^{2+}–citrate complex gradually decomposes, releasing Ca^{2+} into the solution. The crystal nuclei formed at this stage. The formation of dandelions was earlier when hydrothermal for 1 h, which indicated a weak interaction force between Ca^{2+} and citrate. The nanorod units of dandelion crystals can be well grown after further hydrothermal treatment.

3.3. Thermal stability

High-temperature stability was one of the key factors in determining the application of HAP. Therefore, XRD was conducted to test the phase purity of two samples PSC-HAP and TSC-HAP, which were calcined at 800 °C for 6 h. The diffraction peaks of two samples PSC-HAP-800 and TSC-HAP-800 can be indexed as a pure phase of hydroxyapatite (Fig. 7), which coincides well with the standard data for hydroxyapatitie (JCPDS No. 09-0432). No peaks from other calcium phosphates were observed in this XRD pattern, indicating a good stability of the obtained samples at high temperature. It is worth pointing out that there is a large difference from sample TSC-HAP, the broader diffraction peaks based on (1 1 2), (2 1 1) and (3 0 0) became sharper and distinguishable peaks. After thermal calcination, these two kinds of morphologies of HAP can almost be sustained. HAP flowers can be intactly kept upon calcination (Fig. 8a). However, from a high-magnification image (Fig. 8b), one can see the presence of nanopores in the building units of nanosheets. TSC-HAP-800 still possesses morphology of dandelions (Fig. 8c and d). The nanorods on dandelion surface seem to be rough and have a tendency to be melted.

3.4. Drug release property

We investigated the drug loading and release behavior of hierarchical HAP crystals. A typical anti-inflammatory drug, ibuprofen, was used for drug loading. The ibuprofen storage in PST-HAP flowers and TSC-HAP dandelions reached 227.5 and 193 mg/g, respectively.

We also investigated the release behavior of HAP crystals. The released ibuprofen concentration in simulated body fluid was calculated using:

$$y = 0.00173 + 1.7237x \quad (1)$$

where y represents the absorbance value and x represents the ibuprofen concentration in SBF. The total amount of ibuprofen released was calculated using:

$$m_t = C_t \cdot V + v \cdot \sum_{0}^{t-1} C_t \quad (2)$$

where m_t represents total mass of released ibuprofen after taking out release medium solution (v mL) t times; c_t represents

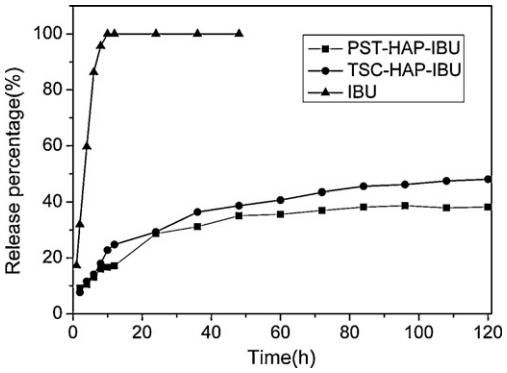

Fig. 9. In vitro IBU release curves of IBU, PST-HAP-IBU and TSC-HAP-IBU in SBF (pH 7.4).

the ibuprofen concentration in SBF at time t; V represents the total volume of SBF and v represents the volume of release medium solution taken out for analysis each time.

Fig. 9 shows the release behavior of pure ibuprofen disk and two kinds of ibuprofen-loaded HAP disk in SBF over a time period of 48 h and 120 h. One can see that the pure ibuprofen disk released much faster and the release finished within 10 h. In contrast, two kinds of ibuprofen loaded HAP disks showed a slow and sustained release of ibuprofen, which can avoid the explosive release of ibuprofen and prolong the drug effect. The drug release rates from two systems are similar in the medium of SBF with pH 7.4. For ibuprofen-loaded PST-HAP flowers, about 29% of the loaded drug was released for the first 24 h and 35% for 48 h, and then the drug release rate reached a value 38% for 120 h. Similarly, for ibuprofen-loaded TSC-HAP dandelions, about 29% of the loaded drug was released for the first 24 h and reached 48% for 120 h. The ibuprofen release was governed by a diffusion process in the initial stage. The ibuprofen was not released completely. This may be explained by the formation of hydrogen bonds between –COOH groups of ibuprofen and –OH groups of HAP crystals, which slow or hold back the release of loaded ibuprofen. The hierarchical HAP crystals as drug carriers can exhibits more effectiveness in assuaging the initial burst release and achieving the sustained release in comparison with pure ibuprofen disk.

4. Conclusion

We have successfully developed a complexing-agent regulated hydrothermal method to prepare hierarchically HAP microspheres assembled by nanosheets and nanorods, respectively. Hierarchical microspheres assembled by the nanosheets have been successfully prepared by a hydrothermal method using PST as complexing agent at 180 °C for 24 h. Well-crystallized HAP dandelions with nanorods radiating from the center can be obtained by the introduction of TSC. Due to complexing effect, less free Ca^{2+} concentration can avoid direct chemical precipitation and hence greatly influence crystal growth process. A typical anti-inflammatory drug, ibuprofen, was used for drug loading, and the release behaviors of ibuprofen in a simulated body fluid were studied. Ibuprofen could be stored in these hierarchically HAP crystals with an uptake amount of 227.5 and 193 mg/g for HAP flowers and dandelions, respectively. HAP flowers and dandelions showed a favorable sustained release property for ibuprofen; thus, they are very promising for application in drug delivery.

Acknowledgements

The authors are grateful for the financial support by the Applied Project of Yantai City (No. 2008308), the Natural Science Foundation of Ludong University (No. LY20072901), National Natural Science Foundation of China (No. 20904018), the Project of Shandong Province Higher Educational Science and Technology Program (J10LF02) and the Foundation of Innovation Team Building of Ludong University (08-CXB001).

References

[1] S. Mann, Molecular recognition in biomineralization, Nature 332 (1988) 119–124.
[2] F. Rahimi, B.T. Maurer, M.G. Enzweiler, Coralline hydroxyapatite: a bone graft alternative in foot and ankle surgery, J. Foot Ankle Surg. 36 (1997) 192–203.
[3] A.N. Hayati, H.R. Rezaie, S.M. Hosseinalipour, Preparation of poly(3-hydroxybutyrate)/nano-hydroxyapatite composite scaffolds for bone tissue engineering, Mater. Lett. 65 (2011) 736–739.
[4] A. Wang, X. Ma, Y. Lu, B. Jiang, R. Zhu, Preparation & characterization and chromatographic property of hydroxyapatite microspheres, J. Chin. Ceram. Soc. 38 (2010) 468–471.
[5] R.V. Suganthi, K. Elayaraja, M.I.A. Joshy, V.S. Chandra, E.K. Girija, S.N. Kalkura, Fibrous growth of strontium substituted hydroxyapatite and its drug release, Mater. Sci. Eng. C 31 (2011) 593–599.
[6] M. Enayati, H. Mobedi, H. Mirzadeh, Effect of nano-hydroxyapatite on controlled release of leuprolide acetate from in situ-forming PLGA implant, J. Pharm. Pharmacol. 60 (2008) A13.
[7] S.H. Teng, E.J. Lee, P. Wang, S.H. Jun, C.M. Han, H.E. Kim, Functionally gradient chitosan/hydroxyapatite composite scaffolds for controlled drug release, J. Biomed. Mater. Res. B 90B (2009) 275–282.
[8] M.Y. Ma, Y.J. Zhu, L. Li, S.W. Cao, Nanostructured porous hollow ellipsoidal capsules of hydroxyapatite and calcium silicate: preparation and application in drug delivery, J. Mater. Chem. 18 (2008) 2722–2727.
[9] K. Kandori, S. Oda, M. Fukusumi, Y. Morisada, Synthesis of positively charged calcium hydroxyapatite nano-crystals and their adsorption behavior of proteins, Colloid Surf. B 73 (2009) 140–145.
[10] J. Tan, M. Chen, J. Xia, Water-dispersible hydroxyapatite nanorods synthesized by a facile method, Appl. Surf. Sci. 255 (2009) 8774–8779.
[11] I.S. Neira, Y.V. Kolen'ko, O.I. Lebedev, G.V. Tendeloo, H.S. Gupta, F. Guitián, M. Yoshimura, An effective morphology control of hydroxyapatite crystals via hydrothermal synthesis, Cryst. Growth Des. 9 (2009) 466–474.
[12] B. Jokić, M. Mitrić, V. Radmilović, S. Drmanić, R. Petrović, D. Janaćković, Synthesis and characterization of monetite and hydroxyapatite whiskers obtained by a hydrothermal method, Ceram. Int. 37 (2011) 167–173.
[13] K. Teshima, S.H. Lee, M. Sakurai, Y. Kameno, K. Yubuta, T. Suzuki, T. Shishido, M. Endo, S. Oishi, Well-formed one-dimensional hydroxyapatite crystals grown by an environmentally friendly flux method, Cryst. Growth Des. 9 (2009) 2937–2940.
[14] C. Huang, Y.B. Zhou, Z.M. Tang, X. Guo, Z.Y. Qian, S.B. Zhou, Synthesis of multifunctional Fe_3O_4 core/hydroxyapatite shell nanocomposites by biomineralization, Dalton Trans. 40 (2011) 5026–5031.
[15] J. Zhan, Y.H. Tseng, J.C.C. Chan, C.Y. Mou, Biomimetic formation of hydroxyapatite nanorods by a single-crystal-to-single-crystal transformation, Adv. Funct. Mater. 15 (2005) 2005–2010.
[16] H.C. Park, D.J. Baek, Y.M. Park, S.Y. Yoon, Thermal stability of hydroxyapatite whiskers derived from the hydrolysis of α-TCP, J. Mater. Sci. 39 (2004) 2531–2534.

[17] K. Furuichi, Y. Oaki, H. Imai, Preparation of nanotextured and nanofibrous hydroxyapatite through dicalcium phosphate with gelatin, Chem. Mater. 18 (2006) 229–234.
[18] M.G. Ma, Y.J. Zhu, J. Chang, Monetite formed in mixed solvents of water and ethylene glycol and its transformation to hydroxyapatite, J. Phys. Chem. B 110 (2006) 14226–14230.
[19] L.X. Yang, Y.J. Zhu, H. Tong, Z.H. Liang, W.W. Wang, Hierarchical β-$Ni(OH)_2$ and NiO carnations assembled from nanosheet building blocks, Cryst. Growth Des. 7 (2007) 2716–2719.
[20] J. Yuan, K. Laubernds, Q. Zhang, S.L. Suib, Self-assembly of microporous manganese oxide octahedral molecular sieve hexagonal flakes into mesoporous hollow nanospheres, J. Am. Chem. Soc. 125 (2003) 4966–4967.
[21] Y. Wang, M.S. Hassan, P. Gunawan, R. Lau, X. Wang, R. Xu, Polyelectrolyte mediated formation of hydroxyapatite microspheres of controlled size and hierarchical structure, J. Colloid Interface Sci. 339 (2009) 69–77.
[22] X. Xiao, R. Liu, C. Qiu, D. Zhu, F. Liu, Biomimetic synthesis of micrometer spherical hydroxyapatite with β-cyclodextrin as template, Mater. Sci. Eng. C 29 (2009) 785–790.